Available online at www.sciencedirect.com
SCIENCE DIRECT®
Acta Materialia 53 (2005) 3961–3970
Acta MATERIALIA
www.actamat-journals.com

Phase equilibria among α-Fe(Al, Cr, Ti), liquid and TiC and the formation of TiC in Fe_3Al-based alloys

Satoru Kobayashi [a,b,*], André Schneider [b], Stefan Zaefferer [a], Georg Frommeyer [b], Dierk Raabe [a]

[a] *Department of Microstructure Physics and Metal Forming, Max Planck Institute für Eisenfoschung, Max-Planck-Str. 1, D-40237 Düsseldorf, Germany*
[b] *Department of Materials Technology, Max Planck Institute für Eisenfoschung, Max-Planck-Str. 1, D-40237 Düsseldorf, Germany*

Received 21 January 2005; received in revised form 29 April 2005; accepted 30 April 2005
Available online 1 July 2005

Abstract

In the context of the development of high-strength Fe_3Al-based alloys, phase equilibria among α-Fe(Al, Cr, Ti), liquid and TiC phases in the Fe–Al–Cr–Ti–C quinary system and the formation of TiC were determined. A pseudo-eutectic trough ($L \Longleftrightarrow \alpha + L + TiC$) exists at 1470 °C at around Fe–26Al–5Cr–2Ti–1.7C on the vertical section between Fe–26Al–5Cr (α) and Ti–46C (TiC) in at.%. Large faceted TiC precipitates form from the melt after the formation of primary α phase even in hypoeutectic alloys. The TiC formation is thought to be due to the composition change of the liquid towards the hypereutectic compositions by solidification of the primary α. In order to remove the faceted TiC, which are unfavourable for strengthening the material, two different processing routes have been successfully tested: (i) solidification with an increased rate to reduce the composition variation of the liquid during solidification, and (ii) unidirectional solidification to separate the light TiC precipitates from the melt.

Keywords: Iron aluminides; Solidification microstructure; Precipitation; Isothermal heat treatment; Thermomechanical processing

1. Introduction

Fe_3Al-based alloys with B2- or $D0_3$-ordered structures are considered to be promising structural materials for high-temperature applications due to excellent high-temperature corrosion resistance in oxidising and sulphidising atmospheres [1], low materials costs and relatively low density compared to steels [2,3]. One of the major obstacles in bringing these alloys into application is their poor ductility at low temperatures. Generally, their brittleness is considered to be due to reactions of the material with hydrogen (hydrogen embrittlement) [3]. However, it was found that the embrittlement can be reduced by alloying with Cr [4,5]. It is also reported that appropriate thermomechanical treatments to achieve deformed and well-recovered states can reduce the embrittlement [6], but this improvement can be lost if recrystallisation occurs during a subsequent heat treatment at high temperatures [6,7]. Consequently, the addition of Cr should be considered as an important factor for alloy design of cast and wrought Fe_3Al-based alloys.

Another still unsolved problem is the poor high-temperature strength and creep resistance of Fe_3Al-based alloys above 600 °C [2,3]. An effective method for the improvement of high-temperature strength is to introduce finely distributed precipitates that are thermodynamically stable at high temperatures. MC-carbides (M = Ti, V, Nb, and Ta), perovskite-type κ-phase (Fe_3AlC_x), Laves phases ($(Fe,Al)_2Ti$, $(Fe,Al)_2Nb$),

* Corresponding author. Tel.: +49 211 6792 321; fax: +49 211 6792 333.
E-mail address: kobayashi@mpie.de (S. Kobayashi).

1359-6454/$30.00
doi:10.1016/j.actamat.2005.04.044

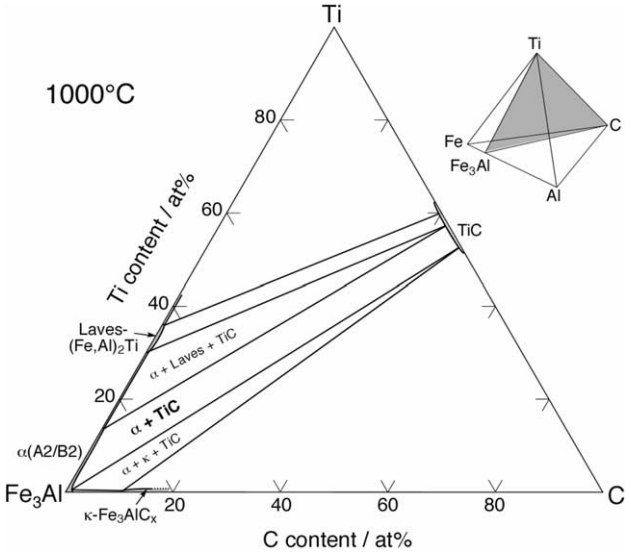

Fig. 1. Schematic drawing of an isothermal section of Fe_3Al–Ti–C at 1000 °C of the Fe–Al–Ti–C quaternary system, based on recent studies [15] and on the literature [16–18].

borides and oxides have all been shown to be useful in strengthening of Fe_3Al-based alloys [8–14].

Schneider et al. [9,10,15] have performed studies on the constitution and microstructures of Fe_3Al-based alloys with MC-carbides, Laves phases and κ-phase. The phase relationships between these precipitates and the Fe_3Al-based matrix phase (hereafter this matrix phase is denoted as α) can be best illustrated by an isothermal section of a Fe_3Al–M–C subsystem in the Fe–Al–M–C (M = Ti, V, Nb, and Ta) quaternary system. Fig. 1 schematically shows an isothermal section of the Fe_3Al–Ti–C quaternary system at 1000 °C, which is drawn based on recent results on phase equilibria in this system [15] and on data concerning phase equilibria in the ternary and binary subsystems [16–18]. The two-phase regions of $\alpha + (Fe,Al)_2Ti$, $\alpha + TiC$ and $\alpha + Fe_3AlC_x$ appear in this order as the Ti/C ratio decreases. This isothermal section thus allows for the required precipitate phases to be chosen by selecting a certain Ti/C ratio.

In the present study TiC was chosen as a precipitate phase for example, and phase equilibria among α-Fe(Al, Cr, Ti), L and TiC phases in Fe_3Al-based alloys at elevated temperatures were determined. The kinetics of the TiC formation during liquid–solid and solid–solid transformation was studied in view of the development of novel Fe_3Al-based alloys with strengthening MC carbides.

2. Experimental procedure

The compositions of the Fe–(26–25)Al–5Cr–(0–3)Ti–(0–2.5)C (at.%) alloys investigated in this study are listed in Table 1 (hereafter all compositions are given in atomic per cent unless specified otherwise). Similar Ti/C ratios (1.2–1.5, see Table 1) were selected in a way that the alloys belong to one tie-line between Fe–26Al–5Cr and TiC at 1450 °C, which was determined in this paper. These alloys were produced as 2 kg ingots by induction melting under an argon atmosphere. The starting materials used are as follows: electrolytic iron of 3 N purity, electrolytic aluminium of 4 N purity, chromium, sponge titanium of 4 N purity and carbon. The Fe–26Al–5Cr is the base alloy and the other alloys are denoted with respect to their Ti and C concentrations in this paper. The ingots were cut to rectangular samples of $8 \times 8 \times 15$ mm in size and heat-treated in air at various temperatures of 600–1550 °C, followed by water quenching. For the heat treatments above the melting temperature, the samples were put in small Al_2O_3 crucibles.

The heat-treated samples were cut into halves and the cross-sections were ground, mechanically polished with diamond paste down to 3 μm, and finally polished with SiO_2 oxide polishing suspension (OPS). The microstructures were examined by optical microscopy and high resolution scanning electron microscopy (HRSEM), which is equipped with a backscattered electron detector. The phases present were identified by electron backscattered diffraction (EBSD) pattern analysis. The compositions of the phases were determined by electron probe micro analyses (EPMA). For the analyses, calibration curves were made to correlate the intensities of Fe, Al, Cr and Ti with their compositions by using several as-cast alloys as standards with the assumption that the nominal compositions and the alloy compositions are equal. The carbon contents were determined by subtracting the compositions of the substitutional elements from 1: $x_C = 1 - (x_{Fe} + x_{Al} + x_{Cr} + x_{Ti})$. More than 10 measurements were performed for each phase and the average values were determined.

Differential thermal analysis (DTA) was performed to determine the transition temperatures of the base alloy and of those with low amounts of Ti and C. The measurements were performed in an argon atmosphere with different heating/cooling rates of 2 and 10 K/min. The liquidus and solidus temperatures were

Table 1
The nominal compositions of the alloys studied (compositions are given in atomic per cent)

Designation	Ti/C ratio	Bulk alloy composition (at.%)				
		Fe	Al	Cr	Ti	C
Base	–	Bal.	26.0	5.0	–	–
0.1Ti–0.07C	1.4	Bal.	26.0	5.0	0.1	0.07
0.3Ti–0.2C	1.5	Bal.	26.0	5.0	0.3	0.2
1.5Ti–1.0C	1.5	Bal.	25.6	5.0	1.5	1.0
2.3Ti–1.9C	1.2	Bal.	25.3	4.8	2.3	1.9
2.9Ti–2.4C	1.2	Bal.	24.8	4.7	2.9	2.4

evaluated by linear extrapolation of the onset temperatures of the melting during heating and of solidification during cooling towards zero heating/cooling rates, respectively.

3. Results and discussion

3.1. Microstructures of the heat-treated and quenched specimens and phase identification

Fig. 2 shows optical micrographs of the 1.5Ti–1.0C alloy heat-treated above the melting temperature and subsequently water quenched. In the specimen heat-treated at 1550 °C, small primary α dendrites few tens of μm in size are observed (Fig. 2(a)). The dark interdendritic regions exhibit rod-like eutectic microstructures, as shown in a high magnification SEM image (Fig. 2(b)). In contrast, a specimen heat-treated at 1470 °C for 1 h after cooling from 1550 °C, exhibits large α dendrites with a size of more than 200 μm besides regions with small dendrites (Fig. 2(c), for comparison see also Fig. 2(a)). The difference in the dendrite size of these two specimens clearly demonstrates that the small dendrites and eutectic regions have been formed from the melt during water quenching, while the larger α dendrites formed at the heat treatment temperature. It is thus obvious that the 1.5Ti–1.0C alloy is in the liquid single-phase region at 1550 °C and in the two-phase region of L + α at 1470 °C.

Fig. 3 shows micrographs of the 1.5Ti–1.0C alloy which was cooled from the L single-phase region to 1450 °C and held for 1 h. Two different morphologies of precipitates – large faceted and fine ones – were observed in the α matrix which is surrounded by small dendrites and eutectic regions (Fig. 3(a)). EBSD measurements revealed that Kikuchi patterns from both the large faceted and fine precipitates correspond to those of TiC with B1 (NaCl) structure (Fig. 3(b) and (c)). The fine TiC precipitates are also observed in larger dendrites of a specimen heat-treated at 1470 °C (Fig. 2(c)). Their fine size and its independence on the heat treatment temperature, indicates that the fine TiC precipitates formed in the α matrix during quenching. The Bain-type crystallographic relationship was found between the α matrix and the fine TiC precipitates: $(0\,0\,1)_{\alpha}//(0\,0\,1)_{TiC}$, $[1\,1\,1]_{\alpha}//[1\,1\,0]_{TiC}$. This result also indicates that the fine TiC precipitates form in the solid state.

The change with time (1 to 60 min) of the area fractions of (i) the small dendrites and eutectic region (both belonging to L at high temperature), (ii) the large dendrites including fine TiC precipitates (α) and (iii) the large faceted TiC precipitates, were measured using a minimum of five optical micrographs taken at a low magnification. The obtained results are shown in Fig. 4. The fraction of the L region decreases while that of α and the large faceted TiC precipitates regions increase with heat treatment time. All the phase fractions

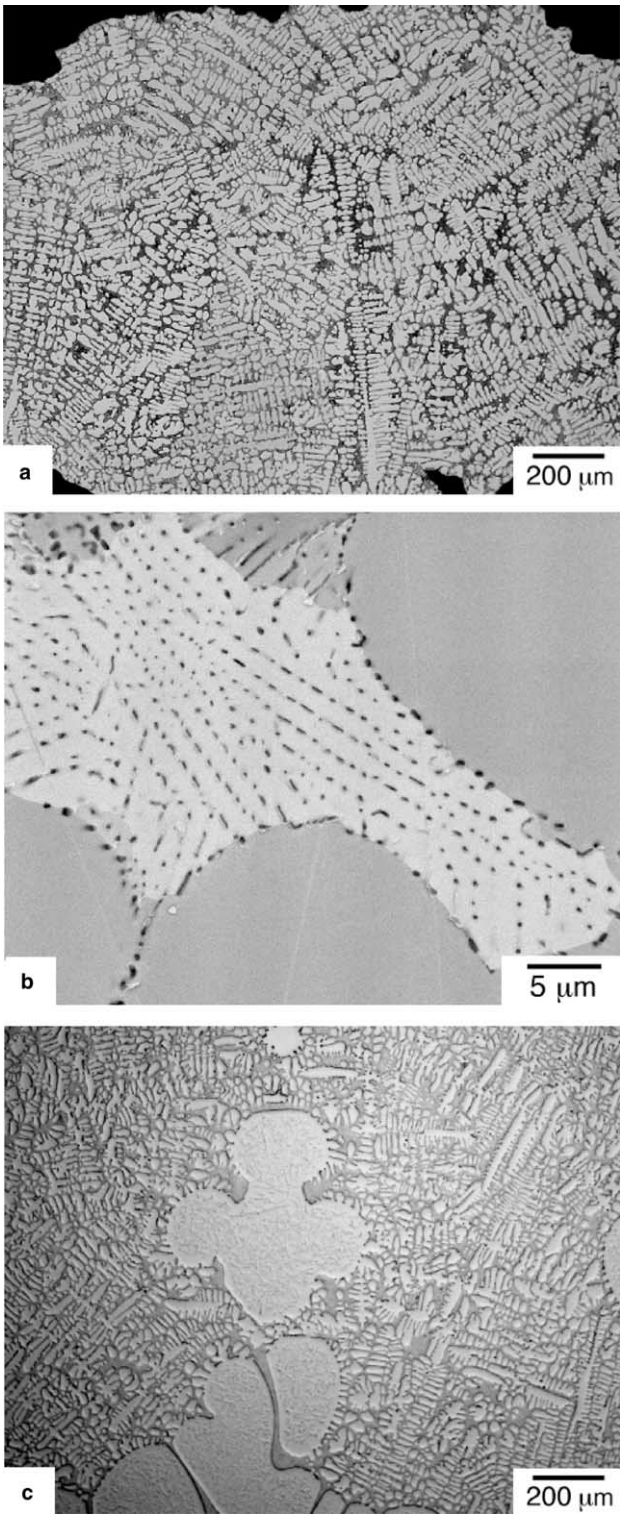

Fig. 2. Microstructures of the 1.5Ti–1.0C alloy heat-treated at 1550 °C for 10 min (a, b) and 1470 °C for 1 h directly cooled from 1550 °C (c), followed by water quenching: (a, c) optical micrographs, (b) back-scattered electron image.

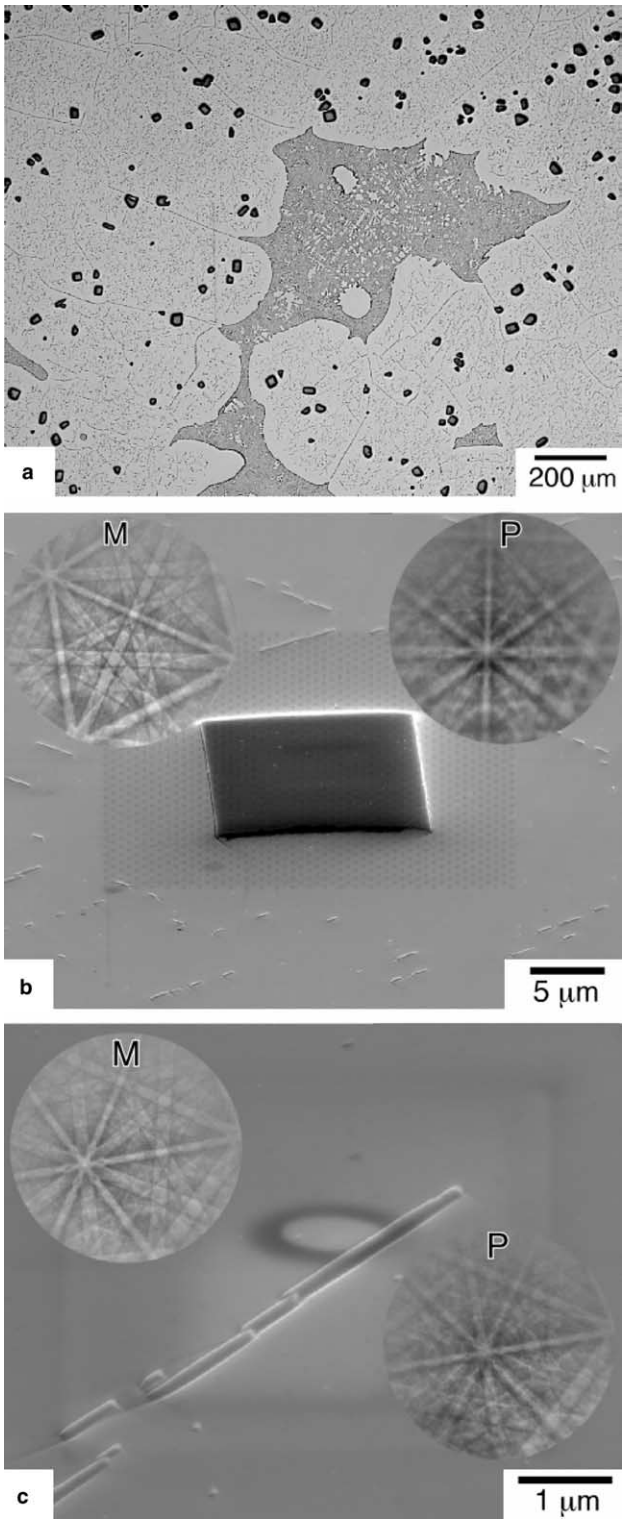

Fig. 3. Microstructures of the 1.5Ti–1.0C alloy cooled from the liquid single-phase region to 1450 °C and held for 1 h (a), together with EBSD Kikuchi-patterns (b, c) of the faceted TiC (b) and fine TiC (c) and α. M stands for matrix, P for precipitates.

are almost saturated after a time period between 10 min and 1 h. This finding leads to the conclusion that a heat treatment time of 1 h is sufficient to reach the equilibrium state at 1450 °C. Thus, it can be stated that the 1.5Ti–1.0C alloy exhibits the L + α + TiC three-phase equilibrium at this temperature. It should be mentioned that the actual fraction of the L and α phases at 1450 °C is not quantitatively reflected by the microstructures investigated at room-temperature, because the L/α interfaces move towards the liquid during quenching.

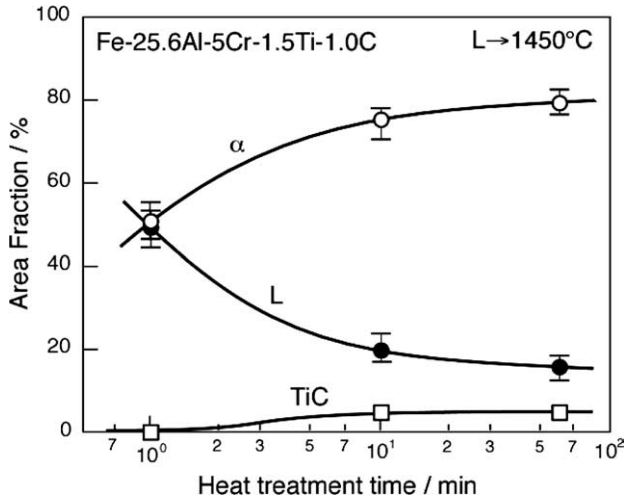

Fig. 4. Change in area fractions of small dendrites and eutectic region (L), large α dendrites containing the fine TiC precipitates (α-Fe), and the faceted TiC with heat treatment at 1450 °C.

3.2. Composition analysis and isothermal section slightly above the melting temperature

The compositions of the liquid, α and TiC phases equilibrated at 1450 °C were determined and the results are listed in Table 2. For the analysis of the L phase composition, X-ray spectra were obtained from centre positions in the regions with small dendrites and eutectic by using scanning mode. The solubility of Ti in α, L and TiC is 0.7%, 2.0% and 54%, respectively. The value of 1.2 for the Ti/C ratio in the TiC phase was obtained. The precision of the analysis for the concentration of C in TiC is quite good with respect to the relevant literature on Fe or Fe_3Al-based alloys [19–21], which report that the Ti/C ratio of the TiC phase depends on the Ti/C ratio in the alloy composition, i.e. the higher is the Ti/C

Table 2
The analysed compositions (in atomic per cent) of the phases present in the 1.5Ti–1.0C alloy heat-treated at 1450 °C for 1 h, followed by water quenching

Phase	Fe	Al	Cr	Ti	C
α	67.9	25.8	5.1	0.7*	0.5
L	64.5	27.0	5.2	2.0	1.3
TiC	0.4**	0.1**	0.3**	53.6	45.6

Deviation for the compositions analysed is within ±1% relative except for: *±7% relative; **±12% relative.

ratio in the alloy composition, the higher it is in the TiC phase. (This can also be understood by regarding the two-phase region of α + TiC in Fig. 1). Note that in Table 2, Fe, Al and Cr are almost completely partitioned to the α and liquid phases and only to a very small extent to the TiC phase. Note that Al is by 1% more partitioned to the liquid than to the α phase, whereas Fe is by ~3% more partitioned to the α phase than the liquid.

According to the composition analysis, the tie-triangle of α + L + TiC at 1450 °C is plotted on the isothermal section with the apices: Fe–5Cr, Al–5Cr and Ti–46C, and shown in Fig. 5. The compositions of the α and L phases on the Fe–Al–Cr ternary edge are referred to the data along the line between Fe–5Cr and Al–5Cr in the literature [22]. The L single-phase region exists on the Al-rich side of the triangle based on the fact that Al is more partitioned to the liquid phase than to the α phase. This result indicates that the tie-triangle moves towards the Al-rich corner with decreasing temperature, which is reasonable with respect to the lower melting temperatures of Al-rich alloys. Consequently, it is assumed that a pseudo-eutectic trough (L → α + L + TiC), which corresponds to the locus of the L composition of the tie-triangle, exists along the Al concentration axis and its temperature decreases with increasing Al exists along the Al concentration axis and shifts to lower temperatures with increasing Al content.

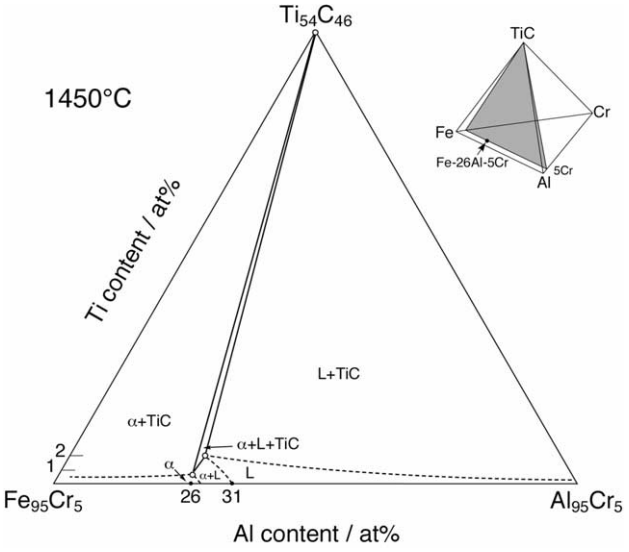

Fig. 5. The tie-triangle of α + L + TiC at 1450 °C plotted on the isothermal section with the apices of Fe–5Cr, Al–5Cr and Ti–46C.

3.3. The vertical section between the phases α and TiC in Fe_3Al-based alloys

Several alloys along the tie-line between the Fe–26Al–5Cr(α) and Ti–46C (TiC) at 1450 °C were produced for experimental determination of the vertical section. Phase equilibria at various temperatures were determined by means of microstructure observations of the

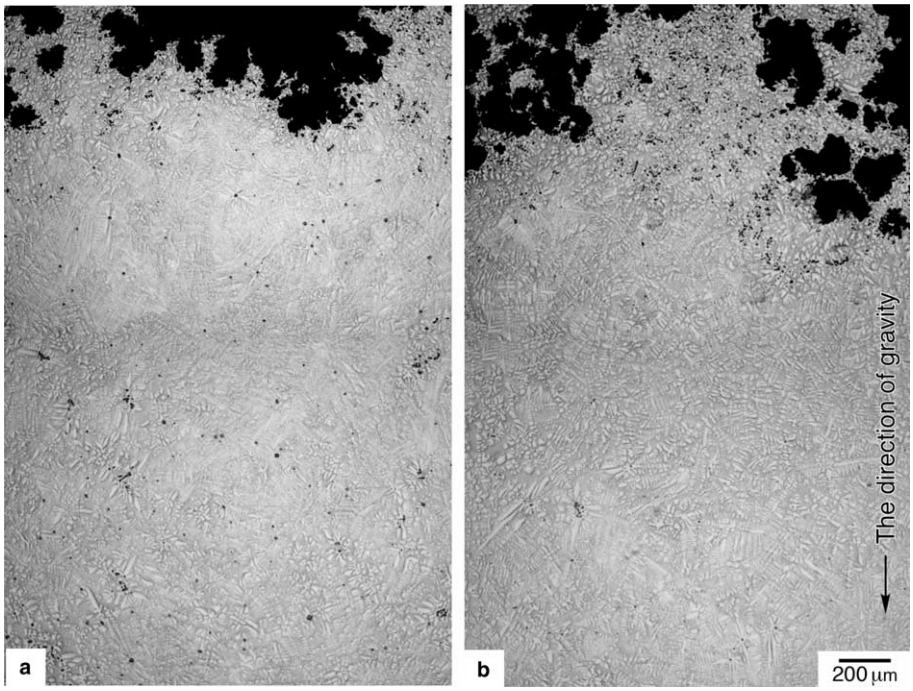

Fig. 6. Optical microstructures of the 2.3Ti–1.9C alloy heat-treated at 1550 °C for 15 min followed by water quenching (a) and subsequently cooled to 1500 °C and held for 15 min followed by water quenching (b). Black dots in the small dendrites region correspond to faceted TiC precipitates. Black part in the top of the specimen is a resin.

heat-treated and quenched samples. With respect to Fig. 6 it is demonstrated how the L and L + TiC phase regions are distinguished in the 2.3Ti–1.9C alloy. Fig. 6(a) shows the microstructures of the alloy heat-treated at 1550 °C for 15 min followed by water quenching and Fig. 6(b) represents the microstructure after cooling from 1550 to 1500 °C and held for 15 min followed by water quenching. Both microstructures exhibit small dendrites and faceted TiC precipitates (black dots). However, the distribution of the TiC precipitates is different apparently. In the specimen heat-treated at 1550 °C the TiC precipitates are homogeneously distributed (Fig. 6(a)), while at 1500 °C TiC precipitates are concentrated at the top part of the specimen (Fig. 6(b)). This result demonstrates that TiC precipitates formed during heat treatment at 1500 °C in the L phase were buoyed up because of the lower density of TiC. However, the TiC precipitates did not form at 1550 °C, but during water quenching. It is therefore a reasonable conclusion that this alloy is in the L single-phase region at 1550 °C and in the two-phase region of L + TiC at 1500 °C. The fact that the TiC forms as a primary phase from the melt also gives us information that this alloy belongs to hypereutectic composition. Table 3 summarises the criteria to discriminate the phase regions at high temperatures from microstructure observations of alloys heat-treated and quenched. Based on these criteria, phase regions at heat treatment temperatures for all the specimens were examined and the results are listed in Table 4.

Fig. 7 shows the part of the vertical section, which possesses Fe–26Al–5Cr on the left hand and the axis with the Ti/C ratio of 1.2–1.5, as determined in this study. The liquidus and solidus temperatures were also determined by DTA for alloys with low Ti and C contents, which are shown in this figure. The section in Fig. 7 can be regarded to represent a quasi-eutectic system. The pseudo-eutectic composition exists around 2.0Ti–1.7C at 1470 °C. The eutectic composition is in good agreement with the composition analysis (Table 2), indicating a reasonable accuracy of the C concentration analysis in the liquid phase. The three-phase coexisting region of α + L + TiC ranges between 1470 and 1450 °C for the quasi-eutectic composition in this section.

Fig. 8 shows the vertical section including the phase boundary between α and α + TiC as determined in this study. The 0.1Ti–0.07C and 0.3Ti–0.2C alloys showed α single-phase at 1300 and 1400 °C but α + TiC two-phase microstructure at 1200 and 1300 °C, respectively (Table 4). These results demonstrate that the phase

Table 3
Criteria to discriminate phase regions at heat treatment temperatures based on microstructure observations

	Microstructural feature	Additional information	Phase region
1	Small dendrites and eutectic· · ·(S)	Hypoeutectic	L
2	(S) and faceted TiC homogeneously distributed	Hypereutectic	L
3	(S) and large dendrites		α + L
4	(S) and faceted TiC concentrated at the top part		L + TiC
5	(S) and large dendrites and faceted TiC		α + L + TiC
6	Single phase	Low supersaturation	α
7	Matrix and fine TiC formed during quenching[a]	High supersaturation	α
8	Matrix and fine TiC formed during heat treatment[b]		α + TiC

[a] The size of the TiC precipitates does not depend on the heat treatment time.
[b] The size of the TiC increases with increasing heat treatment time.

Table 4
Phases present in the alloys heat-treated at high temperatures

Heat treatment conditions	Alloy designation					
	Base	0.1Ti–0.07C	0.3Ti–0.2C	1.5Ti–1.0C	2.3Ti–1.9C	2.9Ti–2.4C
1550 °C/15 min	–	–	–	L	L	L + TiC
1500 °C/15 min	L	L	L	L	L + TiC	–
1480 °C/30 min	–	–	–	–	L + TiC	–
1470 °C/1 h	–	–	–	α + L	–	–
1460 °C/1 h	–	–	–	α + L + TiC	α + L + TiC	L + TiC
1450 °C/1 h	α	α	α	α + L + TiC	α + L + TiC	α + L + TiC
1400 °C/1 h (*)	α	α	α	α + TiC	–	–
1300 °C/1 h	α	α	α + TiC	α + TiC	–	–
* + 1200 °C/2 h	α	α + TiC	α + TiC	α + TiC	–	–
* + 1100 °C/18 h	–	α + TiC	–	–	–	–
* + 1000 °C/18 h	α	α + TiC	–	–	–	–
* + 900–600 °C/18 h	–	α + TiC[a]	–	–	–	–

[a] A2–B2 disorder–order transition is at 824 °C as determined by DTA.

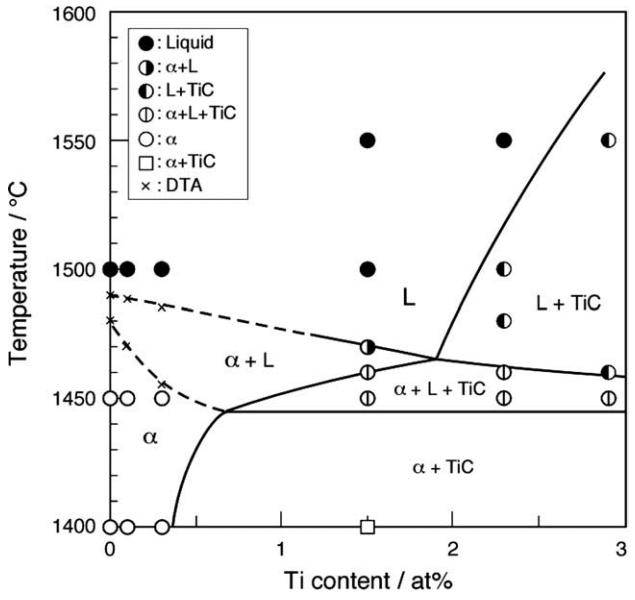

Fig. 7. The vertical section which contains Fe–26Al–5Cr on the left hand and possesses the Ti/C of 1.2–1.5 around the melting temperature.

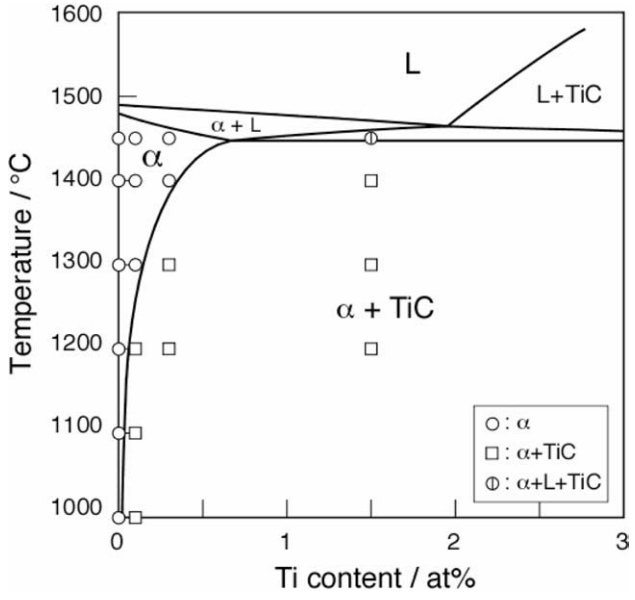

Fig. 8. The vertical section which contains Fe–26Al–5Cr on the left hand and possesses the Ti/C of 1.2–1.5, including the phase boundary between α and α + TiC.

boundary between α and α + TiC exists around 0.3–0.4% at 1400 °C and at less than 0.1% at 1200 °C in this section. Higher solubility of Ti (1%) was reported in Fe–26Al–2Ti–1C heat treated at 1000 °C [9]. The lower solubility of Ti in this study probably results from the lower Ti/C ratio (1.2–1.5) in our alloy compositions than the one in the literature [15]. (Readers are referred to the first paragraph of Section 3.2 and Fig. 1.) In addition, differential thermal analysis peaks for the formation or dissolution of TiC were not detected in the heating/cooling rate range studied here presumably due to their low volume fraction.

3.4. The formation of TiC

3.4.1. TiC formation during liquid–solid transformation

Fig. 9 reveals an as-cast microstructure in the hypoeutectic 1.5Ti–1.0C alloy. The faceted TiC precipitates with a size of 5 μm are observed together with the eutectic TiC precipitates. This type of microstructure was observed in the literature [23], and the formation mechanism was explained as hypereutectic alloys based on conventional wisdom that in hypereutectic alloys the large faceted TiC precipitates form as a primary phase from the melt. However, as clearly presented in the previous chapter, the pseudo-eutectic composition is at around 2.0Ti–1.7C at 1470 °C, indicating that this microstructure is available even in hypoeutectic alloys.

The microstructure evolution of the hypoeutectic 1.5Ti–1.0C alloy was studied by cooling the samples down from the liquid phase to 1450 °C, which is within the three-phase coexisting region of α + L + TiC, and subsequent isothermal ageing. After 1 min ageing (Fig. 10(a)), large α dendrites appear in the region with small dendrites and eutectics, which means that primary α phase starts to form in the liquid at first. On further ageing, the faceted TiC precipitates (designated by arrows) are present in the liquid region at 1450 °C (Fig. 10(b)). After 10 min ageing, the TiC precipitates are observed in the large α dendrite and the size of the TiC increases (Fig. 10(c)). These results clearly demonstrate that the faceted TiC precipitates were formed in the liquid during ageing after the formation of the primary α dendrites, and then surrounded by the α phase with further ageing. The heat treatment did not cause any significant change of the size of the eutectic structure, indicating that the

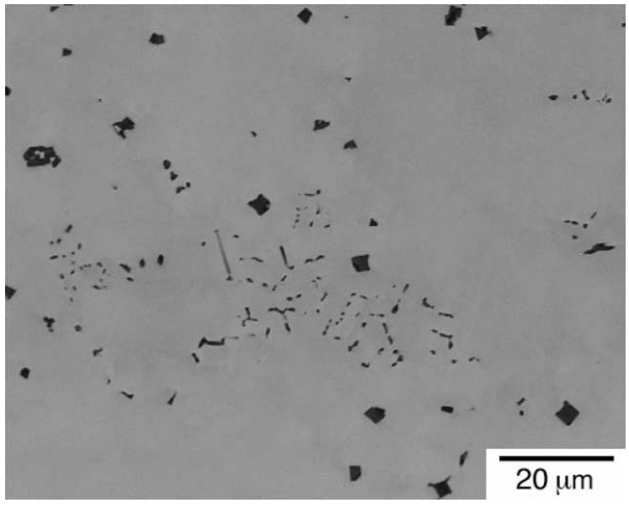

Fig. 9. Backscattered electron image showing the as-cast microstructure of the hypoeutectic 1.5Ti–1.0C alloy.

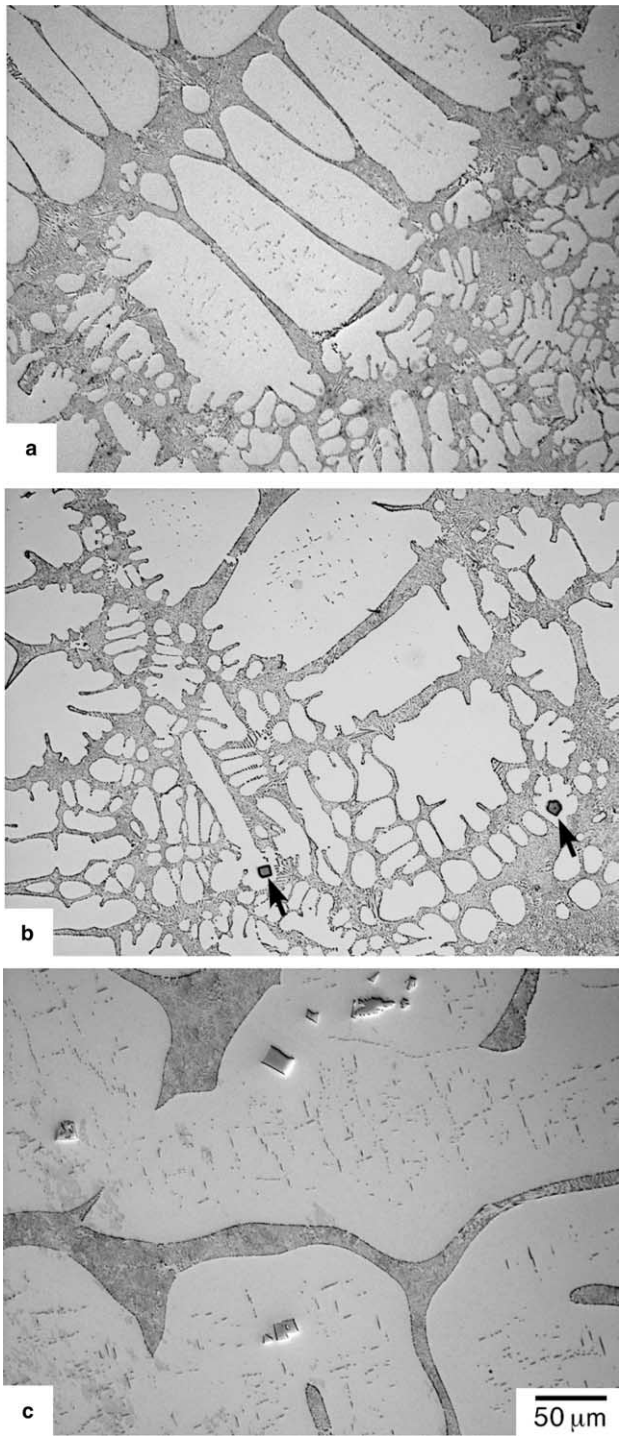

Fig. 10. The change in microstructure of the hypoeutectic alloy cooled from liquid single-phase region and isothermally aged at 1450 °C followed by water quenching. Magnification is the same for all photographs.

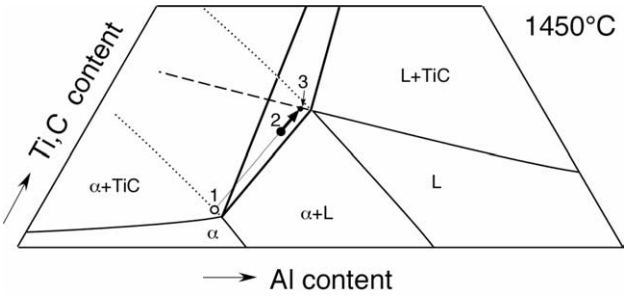

Fig. 11. Schematic illustration of the microstructure evolution in a hypoeutectic alloy along the transformation pathway of L → α + L + TiC; 1: metastable primary α phase, α_m, 2: alloy composition, 3: the composition at which supersaturation starts to occur with respect to the TiC formation in the liquid phase.

eutectic transformation starts to occur below 1450 °C. However, the transformation temperature is not yet precisely determined.

Fig. 11 shows a schematic illustration of the microstructure evolution in a hypoeutectic alloy along the transformation pathway of L → α + L + TiC. The initial composition (point 2) is supersaturated only with respect to the α phase formation. However, the liquid phase composition changes towards the Ti and C rich concentration by solidification of the primary α phase (point 1). Once the composition crosses the metastable phase boundary of L/L + TiC (point 3), the supersaturation of the solute elements in the liquid phase occurs with respect to the TiC formation. In this stage, it is possible for TiC to form in the liquid. When the TiC carbide precipitates, the Ti and C concentration in the liquid phase will be depleted in the vicinity of the TiC, which makes the primary α phase grow easily around the faceted TiC. Based on this discussion, the formation of the as-cast microstructure in hypoeutectic alloys can be described as follows: L → L + α primary dendrite → L + α + faceted TiC → eutectic (α + TiC) + α + faceted TiC.

Strengthening by fibre- or lamellar-like eutectic precipitates is of interest for cast alloy developments. However, the formation of the faceted TiC precipitates is detrimental to the mechanical properties. In the following, two procedures for getting rid of the detrimental TiC precipitates will be shown. For hypoeutectic alloys one procedure is based on rapid cooling in order to avoid the supersaturation with respect to TiC formation, i.e., when the composition of the liquid ranges between the point 2 and 3 (see Fig. 11). Fig. 12 exhibits an optical micrograph of the hypoeutectic alloy air-cooled from the melt. Here, only a few faceted TiC precipitates were observed. Note that the area fraction of the eutectic region increases by quick cooling. The reason for this increase is possibly due to the higher Ti and C content of the liquid phase, owing to the fact that the formation of the faceted TiC precipitates was suppressed.

Another method to remove the faceted carbides is to make use of gravitational segregation. Fig. 13 shows a top part of the longitudinal section of the hypereutectic 2.3Ti–1.9C alloy unidirectionally solidified with a

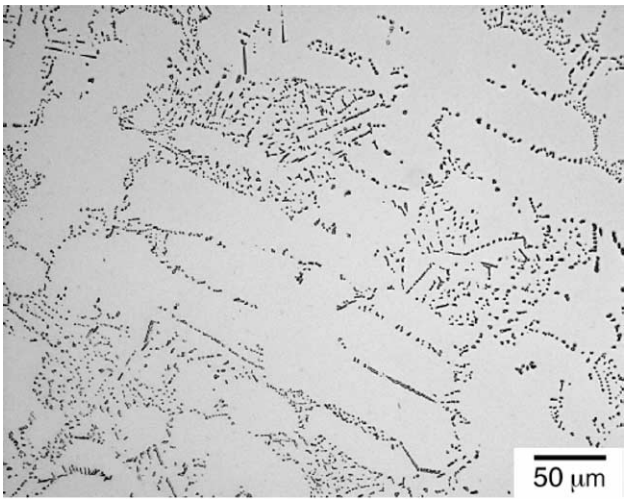

Fig. 12. Optical micrograph of the hypoeutectic 1.5Ti–1.0C alloy cooled in air from 1550 °C, showing no faceted TiC.

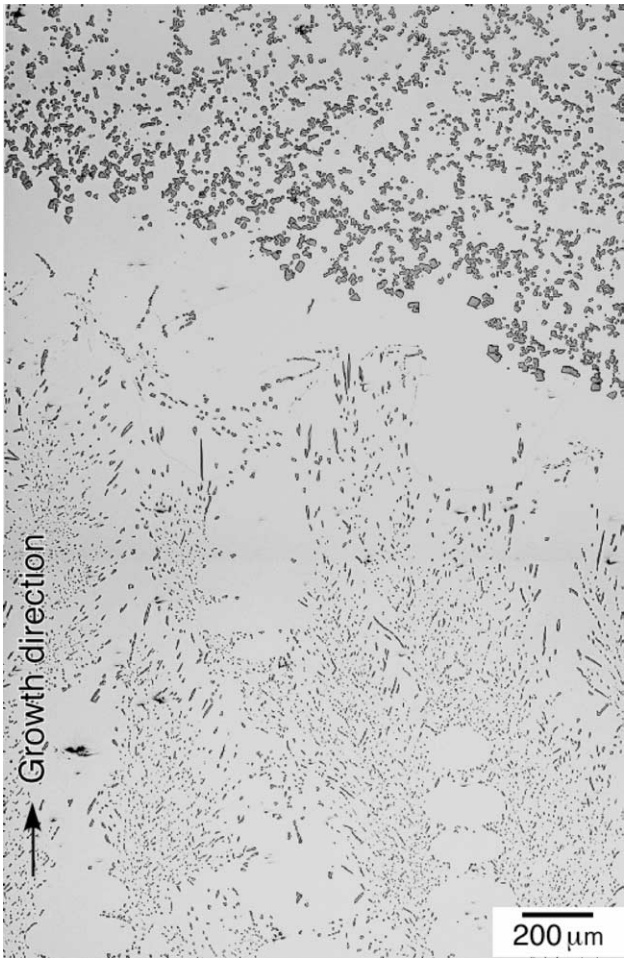

Fig. 13. Optical microstructure showing the longitudinal section of the 2.3Ti–1.9C alloy unidirectionally solidified with a growth rate of 10 mm/h. The vertical direction corresponds to the solidification direction as well as the direction of gravity.

growth rate of 10 mm/h. The faceted TiC precipitates are only observed in the very top part of the specimen, but not in the balance of the specimen. In the lower part, eutectic TiC precipitates are formed between primary dendrites (α) aligned along the growth direction. The evolution of the segregated microstructure can be explained as follows: the faceted TiC precipitates formed in the liquid phase, first and rise to the top due to their lower density in relation to the melt, followed by the formation of the primary α phase and eutectic.

3.4.2. TiC formation during solid–solid transformation

The kinetics of TiC precipitation in the solid state were investigated for alloys with low Ti and C contents. Fig. 14 shows a TTT diagram for TiC precipitation in the α phase for the 0.1Ti–0.07C and 0.3Ti–0.2C alloys. The 0.1Ti–0.07C alloy was homogenised in the α single-phase region and then isothermally aged between 1200 and 600 °C. The existence of the TiC precipitates was checked by high resolution SEM. The TTT curve exhibits C shape and the nose of the C curve is around 950 °C at few tens of seconds. In the 0.3Ti–0.2C alloy, precipitation occurs even during water quenching after homogenisation in the α single-phase region, indicating the very fast precipitation kinetics. This fact makes it difficult to control precipitation reaction by heat treatment in this system, as described and discussed in the following paragraph.

It is desirable in wrought processing that a large volume fraction of precipitates be obtained after hot deformation such as hot rolling and hot extrusion, since a large volume fraction of precipitates can make the deformation processes difficult and would promote recrystallisation; this leads to embrittlement [6,7], in subsequent heat treatments or under service conditions. In fact, we reported that recrystallisation is promoted by a large volume fraction of TiC precipitates during hot

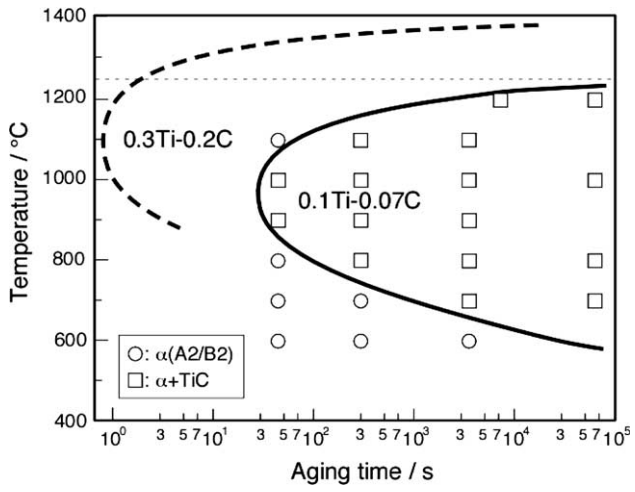

Fig. 14. TTT diagram for the precipitation of TiC in the α phase of the 0.1Ti–0.07C (solid line) and 0.3Ti–0.2C alloys (broken line).

deformation in the 0.3Ti–0.2C alloy [24]. In order to achieve a desirable processing route for this alloy system, heat treatments at very high temperature are necessary to obtain small volume fractions of TiC precipitates, because it is impossible to obtain low volume fraction at low temperatures due to the rapid precipitation kinetics (Fig. 14). However, deformation at high temperature is not desirable in real wrought processing. It is therefore necessary to find other alloy systems where precipitates start to form at lower temperatures and during longer periods to optimise thermomechanical processing; this is discussed elsewhere [24].

4. Conclusions

In the present study, the phase equilibria among α-Fe(Al, Cr, Ti), liquid (L) and TiC phases in Fe_3Al-based alloys and the formation of TiC during liquid–solid and solid–solid transformations were determined based on microstructure observations. The results of this study are as follows:

1. A pseudo-eutectic trough ($L \rightarrow \alpha + L + TiC$) exists at 1470 °C at the composition around Fe–26Al–5Cr–2Ti–1.7C on the vertical section between Fe–26Al–5Cr (α) and Ti–46C (TiC). The eutectic trough temperature decreases with increasing Al concentration.
2. The solubility of Ti in the α phase is around 0.3–0.4% at 1400 °C and less than 0.1% at 1200 °C on this vertical section.
3. Large faceted TiC precipitated from the melt even in hypoeutectic alloys. The formation of the faceted TiC is explained by the change in the composition of L towards the Ti and the C rich side due to the formation of the primary α phase which is lean in Ti and C.
4. In order to avoid the formation of the faceted TiC precipitates, the following methods have been successfully tested.
   (1) High solidification rate to avoid the supersaturation of Ti and C in the L phase for the formation of TiC.
   (2) Unidirectional solidification to make use of gravitational segregation leading to separation of the light TiC precipitates from the melt.
5. The kinetics of the precipitation of TiC in the α phase is very quick, and control of the precipitation reaction in this system is therefore very difficult.

Acknowledgements

The authors thank Mr. K. Markmann and Ms. B. Schaff of the Max-Planck-Institut für Eisenforschung for their experimental assistance. The authors also thank Dr. S. Milenkovic for his fruitful discussions of the results obtained from unidirectional solidification.

References

[1] Klöwer J. In: Grabke HJ et al., editors. Oxidation of intermetallics. Weinheim: Wiley-VCH; 1997. p. 203.
[2] Morris DG. In: Schneibel JH et al., editors. Processing, properties and applications of iron aluminides. Warrendale (PA): TMS; 1994. p. 3.
[3] Stoloff NS. Mater Sci Eng A 1998;258:1.
[4] MacKamey CG, Horton JA, Liu CT. Scripta Metall 1988;22:1679.
[5] MacKamey CG, Horton JA, Liu CT. J Mater Res 1989;4:1156.
[6] MacKamey CG, Pierce DH. Scripta Metall 1993;28:1173.
[7] Huang YD, Yang WY, Chen GL, Sun ZQ. Intermetallics 2001;9:331.
[8] MacKamey CG, Maziasz PJ. In: Schneibel JH et al., editors. Processing, properties and applications of iron aluminides. Warrendale (PA): TMS; 1994. p. 147.
[9] Schneider A, Sauthoff G. Steel Res Int 2004;75:55.
[10] Schneider A, Falat R, Sauthoff G, Frommeyer G. Intermetallics [in press]. Available online 4 May 2005.
[11] Falat R, Schneider A, Sauthoff G, Frommeyer G. Intermetallics [in press]. Available online 26 April 2005.
[12] Morris DG, Morris MA, Baudin C. Acta Mater 2004;52:2827.
[13] Liu CT, George EP, Maziasz PJ, Schneibel JH. Mater Sci Eng A 1998;258:84.
[14] Morris DG, Morris MA. Intermetallics 2000;8:997.
[15] Schneider A, Falat R, Sauthoff G, Frommeyer G. Intermetallics 2003;11:443.
[16] Palm M, Inden G, Thomas N. J Phase Equil 1995;16:209.
[17] Palm M, Inden G. Intermetallics 1995;3:443.
[18] Massalski TB et al., editors. Binary alloy phase diagrams. Metals Park (OH): ASM International; 1990. p. 888.
[19] Subramanian R, Schneibel JH. Mater Sci Eng A 1997;239–240:633.
[20] Raghavan V. J Phase Equil 2003;24:62.
[21] Frage N. Metall Mater Trans 1999;30B:857.
[22] Petzow G, Effenberg G, editors. Ternary alloys, vol. 8. Germany: VCH Verlagsgesellschaft; 1993. p. 324.
[23] Ko SH, Hanada S. Intermetallics 1999;7:947.
[24] Kobayashi S, Zaefferer S, Schneider A, Raabe D, Frommeyer G. Intermetallics [in press]. Available online 9 April 2005.